IOPscience iopscience.iop.org

Home Search Collections Journals About Contact us My IOPscience

Growth behaviour of Ge nano-islands on the nanosized Si{111} facets bordering on two {100} planes

This content has been downloaded from IOPscience. Please scroll down to see the full text.

2006 Nanotechnology 17 5207

(http://iopscience.iop.org/0957-4484/17/20/027)

View the table of contents for this issue, or go to the journal homepage for more

Download details:

IP Address: 140.113.38.11
This content was downloaded on 26/04/2014 at 08:32

Please note that terms and conditions apply.

INSTITUTE OF PHYSICS PUBLISHING NANOTECHNOLOGY
Nanotechnology **17** (2006) 5207–5211 doi:10.1088/0957-4484/17/20/027

Growth behaviour of Ge nano-islands on the nanosized Si{111} facets bordering on two {100} planes

Shyh-Shin Ferng[1], Tsung-Hsi Yang[2], Guangli Luo[3], Kai-Ming Yang[1], Ming-Feng Hsieh[1] and Deng-Sung Lin[1]

[1] Institute of Physics, National Chiao-Tung University, 1001 Ta-Hsueh Road, Hsinchu 300, Taiwan
[2] Microelectronics and Information Systems Research Center, National Chiao-Tung University, Hsinchu 300, Taiwan
[3] National Nano Device Laboratories, 26 Prosperity Road 1, Science-base Industrial Park, Hsinchu 300, Taiwan

E-mail: dslin@mail.nctu.edu.tw

Received 15 June 2006, in final form 10 September 2006
Published 28 September 2006
Online at stacks.iop.org/Nano/17/5207

Abstract
Si(100) substrates were used to fabricate various nanosized {111} facets between the (100) planes using photolithography and anisotropic wet chemical etching. Following simultaneous Ge chemical vapour deposition on the neighbouring (100) and {111} facets, the Ge nano-island formation and distribution was observed on both the (100) terraces and the {111} side walls using a dynamical atomic force microscope. The nano-island formation on the nanosized {111} strip facets was found to be strongly suppressed upon reducing the strip width due primarily to the interaction of adatoms on the neighbouring facets. Specifically, the difference in the effective chemical potential of Ge adatoms on the two neighbouring facets leads to the depletion of nano-islands on the {111} strip with width <500 nm under the growth condition used in this study.

(Some figures in this article are in colour only in the electronic version)

1. Introduction

The strain-driven self-organized growth of the three-dimensional quantum-dot (QD) nanostructure in semiconductor heteroepitaxy has attracted considerable attention [1]. The quantized energy levels in the QDs can be manipulated through controlling their sizes and shapes, producing numerous promising nanoelectronics and optoelectronic devices [2]. In the growth processes and control, Ge-rich nano-island formation on the low-index silicon surfaces represents an ideal system for more thoroughly understanding the nature and the mechanism of the size distribution, evolution, and shape transformation of the QDs.

Nanoscale-sized surfaces in the form of mesas or ridges on patterned substrates offer opportunities not only for novel growth-control engineering, but also for gaining a fundamental understanding of the phenomena of size-dependent crystal growth during the formation of QDs. Nanosized surfaces are confined by boundaries such as growth-resistant thin films, nearly-vertical side walls milled by reactive ion etching (RIE), and well-defined low-index crystalline facets. Shiraki *et al* studied the size effect by depositing Ge on oxidized Si(100) windows with diameters ranging from 90 to 650 nm [3]. Their experimental results demonstrated that Ge size and numbers of Ge nanoislands increase with the window diameter. Similar experiments were performed on the patterned Si(100) square and circular mesas with size ranging from 90 to 580 nm and the sizes and numbers of the Ge nano-islands were found to increase monotonically with the mesa size [3, 4]. Additionally, the nano-islands were found to nucleate preferentially at the mesa edges and corners obtained using RIE [5, 6]; Yang *et al* attributed their observation to the lower chemical potential in these regions resulting from the spatially nonuniform relaxation of the strained wetting layer [5]. Moreover, Jin *et al* showed similar preferential nucleation at the mesa edges

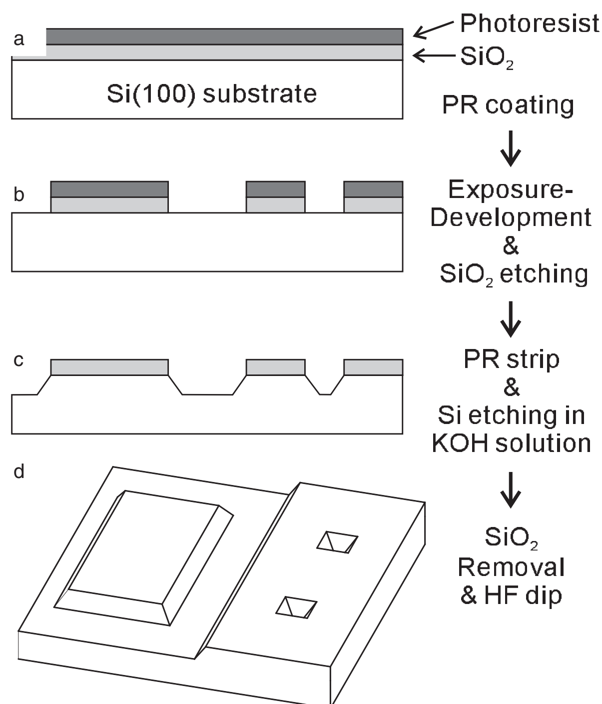

Figure 1. Process flow chart for the fabrication of 2D arrays of rectangular mesas and negative pyramids.

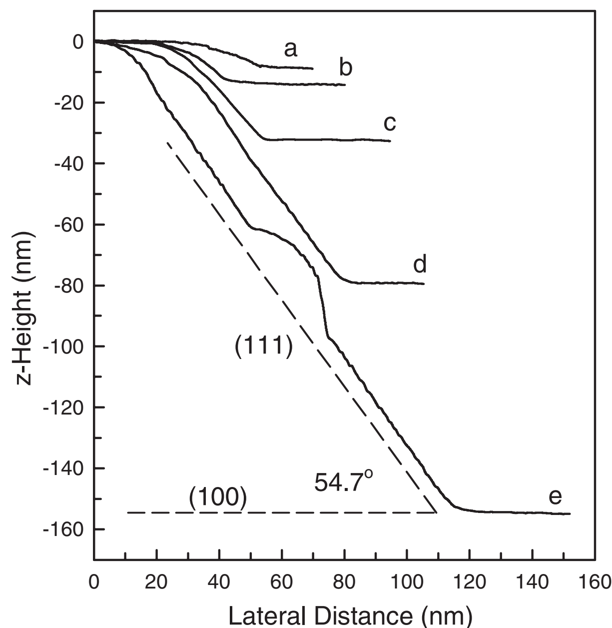

Figure 2. AFM z-height profiles over the mesa side walls following etching in KOH + IPA solution. The etching depth is about (a) 9, (b) 15, (c) 32, (d) 80, and (e) 150 nm. The two dashed lines provide guides to the (100) and {111} planes. The profiles reveal that the {111} facets become well defined as the etching depth exceeds 30 nm. The bump near the centre of (e) was created by scanning over a grown nano-island.

and also that no nano-islands grow on the (113) mesa side walls [7].

As mentioned above, studies of the Ge nano-island growth on the windows or mesas have largely focused on the (100) plane of silicon. Few works have discussed the growth of nano-islands on the nanosized {111} plane. Using tetramethyl ammonium hydroxide (TMAH) solution to fabricate V-groove patterns in the Si(100) substrate with large {111} side walls, Suda *et al* observed that deposited Ge adatoms migrate from the surrounding (100) surface to the bottom of the V-groove or pits and form nano-islands at growth temperatures exceeding 750 K [8]. Olzierski *et al* used TMAH to build nanometre-scale V-grooves with {111} walls on oxidized Si(100) substrate [9]. Their results show that the Ge islands do not grow on the flat {111} facets, but rather nucleate at the bottom of the V-grooves.

This study reports the growth of nano-islands on nanoscale {111} surfaces created via KOH anisotropy etching. The nanoscale surface areas are surrounded by well-defined (100) or {111} planes. The nano-island formation on the small surface areas was found to be strongly dependent on the area geometry. The effect of area geometry was attributed to the adatom flux in or out of the small surface areas into the surrounding plane.

2. Experimental details

Figure 1 illustrates the sample process flow used in the experiment. First, the four-inch n-type Si(100) wafers were RCA cleaned and thermally oxidized to form approximately 100 nm thick SiO_2 films. Using conventional optical photolithography and buffered oxide etch (BOE) solution etching, various rectangular-shaped Si windows with their edges oriented along the [110] direction were then opened. The {111} facets were obtained by etching in stirred 20% KOH + isopropyl alcohol (IPA) (5:1) solution at room temperature for various periods to achieve the desired width [10]. This strong-base solution preferentially etches the {100} and {110} planes, relative to {111}, in single-crystal silicon, thus creating an anisotropic etch. The etching rate along the (100) plane is ~15 nm min^{-1}. Following KOH etching, the SiO_2 masks were removed by BOE etching.

Before patterned Si wafers were loaded into the growth chamber, the substrates were chemically cleaned and dipped into a diluted HF solution to produce a hydrogen-terminated surface. Ge growth was performed via ultra-high vacuum chemical vapour deposition (UHV-CVD) at a growth temperature of 650 °C with a GeH_4 flow rate of 5 sccm. Under the present study conditions, the growth rate is about 2.3 nm min^{-1} on the (100) surface. The samples investigated in this study had a growth time of 100 s, and thus, an average Ge thickness of 3.5 nm. Following growth, the surface topography of the samples and three-dimensional (3D) islands were examined using a commercial atomic force microscope (AFM) operated in tapping mode in air.

3. Results and discussion

3.1. *The formation of well-confined {111} surfaces*

As described in section 2, the flat nanosized Si{111} facets confined by the Si(100) zones were obtained through anisotropic wet chemical etch. The etching time regulates the etching depth and thereby the width of the {111} facets (W_{111}). Figure 2 shows the typical AFM line profiles for

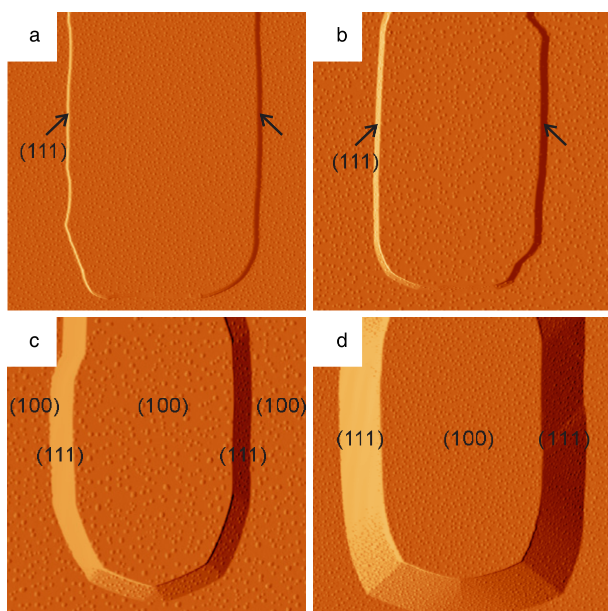

Figure 3. Derivative AFM images displaying Si mesas after Ge growth. The arrows indicate the {111} planes. The width of the {111} facets is about (a) 100, (b) 180, (c) 530, and (d) 1190 nm. Most nano-islands are dome clusters with an average radius of 30 nm and average height of 15.2 nm on the (100) plane. The image sizes are $5.5 \times 5.5\ \mu m^2$.

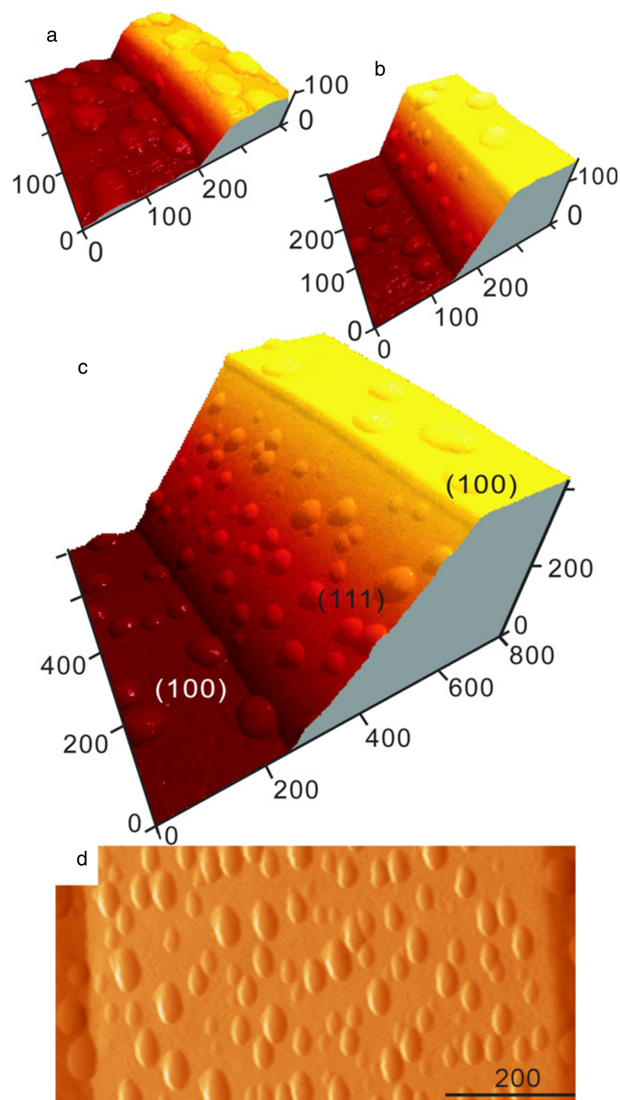

Figure 4. Zoom-in images over the {111} facet for the same samples, namely (a) figure 3(a), (b) figure 3(b), (c) figure 3(c), and (d) figure 3(d). (a)–(c) are three-dimensional images while (d) is a derivative image. The scales are in units of nanometre.

various etching depths from 9 to 150 nm. Based on the basic geometrical analysis of the diamond structure, the angles between the (114), (113), and (111) planes and the (100) plane are 19.5°, 25.3°, and 54.7°, respectively. The evolution of the topographic profiles and overall angles in figure 2 indicates that the (113) and (114) planes are not evident under the wet etching and that the {111} facets become well-defined as the etching depth exceeds ~30 nm.

The bottom boundary of the {111} facets is concave and figure 2 demonstrates that the {111} and (100) facets meet with a sharp angle. In contrast, the top boundary is convex, and the cusp between the {111} and (100) facets is blunt, possibly because of the undercut etch and the balance of the strain relaxation and chemical bonding energy [5].

3.2. Ge nano-islands on the (100) planes

Figure 3 displays the derivative AFM images taken after Ge UHV-CVD growth on the patterned Si(100) samples with various KOH etch time. A mesa is clearly visible near the centre of each image; the photolithographic mask used in patterning the mesas has an area of $3 \times 6\ \mu m^2$. With increasing etch depth, the side walls of the Si(100) mesas expand at the expense of the mesa area. Depending on the relative etching rates of the solution [11], as figure 3 illustrates, the side walls of the etched mesas comprise various crystallographic planes other than the {111} facets discussed in this study.

A 3D island forms a stable nucleus owing to the roughening transition from the stained wetting layer; this is a Stranski–Krastanov growth process. The critical thickness before island formation for Ge growth on Si(100) is known to be around 3 ML for the large (100) areas. Once the critical thickness is exceeded, islands grow in a random manner. Most nano-islands are dome clusters with an average radius of 30 nm, average height of 15.2 nm, and island number density (N_{100}) of $5 \times 10^9\ cm^{-2}$. Compared with a previous study [12], the island number density obtained in this approach is higher and the average size of nano-islands is smaller due to the smaller diffusion length of the Ge adatoms during the higher rate and low-temperature deposition in this work [13]. The island density on the (100) facets appears to be constant throughout their areas in figure 3.

3.3. Ge nano-islands on the {111} planes

In figure 3, the {111} facets fence the left and right sides of the (100) mesas appearing as the bright and dark bands in the image because of the derivative imaging processing. Figure 4 displays typical zoom-in images over these {111} side walls. The {111} facets have width (W_{111}) of around

100, 180, 530, and 1190 nm for figures 4(a)–(d), respectively. These islands ripen during growth, broadening the volume distribution. Presumably these islands consist of the SiGe alloy [17, 15]. Similar to the (100) surface areas, nano-islands appear on the {111} facets once Ge coverage exceeds ∼3–5 ML [14–16]. The average Ge thickness of about 15 ML is much larger than those of the wetting layers; therefore, the slight difference in the wetting layer thickness does not affect the nucleation behaviour observed herein.

On the large {111} facets such as in figures 4(c) and (d), the nano-islands have a smaller average size and a higher number density (N_{111}) compared to those (N_{100}) on their neighbouring (100) facets. The equivalent thickness of the Ge growth obtained by integrating island volume per unit area is roughly the same for both the large {111} and (100) areas. Neglecting the difference in the critical thickness of their wetting layers, the Ge concentration of the wetting layers and islands, the effect of the finite radius of the AFM tip on the island size measurement, and the scanning geometry difference on the two surfaces, this study estimated the deposition rates of Ge on the two facets to be roughly equal, while a similar study showed that the growth rate in {111} is about half of that in (100) [17]. Within the limitations of the AFM resolution, the nano-islands do not show facets as those observed in the molecular beam epitaxy at low rate [18]. This study estimates that N_{111} is $\sim 4N_{100}$. The crystallographic orientations of the two facets in the growth chamber might affect their growth rates slightly, but not their growth morphology under similar growth conditions. The island number density N is roughly proportional to $D^{-1/3}$ at the same deposition rate, where D denotes the diffusion coefficient [19]. The higher island density indicates a smaller diffusion coefficient, that is, $D_{111} \sim D_{100}/60$ on the wetted layers of the two facets.

Compared to the central area in figures 4(c) and (d), N_{111} near the border of the (100) facets is noticeably smaller. In fact, nearly nuclei-free bands (known as the denuded zone) are clearly observable on both edges of the {111} facets in figure 4(c); their width (W_{dz}) is of the order of a few tens of nanometres. When W_{111} is compatible with W_{dz}, both the island density N_{111} and the average sizes of the nano-islands on the {111} facets decrease significantly, as shown in figures 4(a) and (b). In contrast, N_{100} displays little variation between the situations where it is near to and distant from the edges. As shown in figure 5, similar island depletion zones on the {111} planes are also evident in the negative pyramid structure created on a square silicon oxide window on the same substrate as that in figure 3(c).

The reduction in the island density and size on the {111} facets near their border with the (100) facets implies the loss of Ge adatoms on the {111} facets either to a good sink of adatoms at the boundary of the two facets or to the neighbouring (100) facet. Figure 3 and their zoom-in images show that the (100) facet near the convex boundary contains nano-islands; however, few nucleated islands are visible above the convex boundary. Restated, preferential nucleation of nano-islands on the (100) facet near the {111} boundaries is not as evident as near the (100), (110) and a curved surface [20, 5]. The convex edges between the {111} and (100) facets are not good sinks for Ge adatoms. Nevertheless, near the concave boundary (or the L-shape groove), however, preferential nucleation is slightly enhanced on the (100) plane, as shown in figure 4(c). The base areas of these nano-islands are on the (100) plane, indicating that they nucleate on the (100) plane and grow to contact with the V-groove. In comparison, Ge nano-islands preferentially grow on top of the V-grooves between two {111} family planes (figure 5) [17, 8, 9].

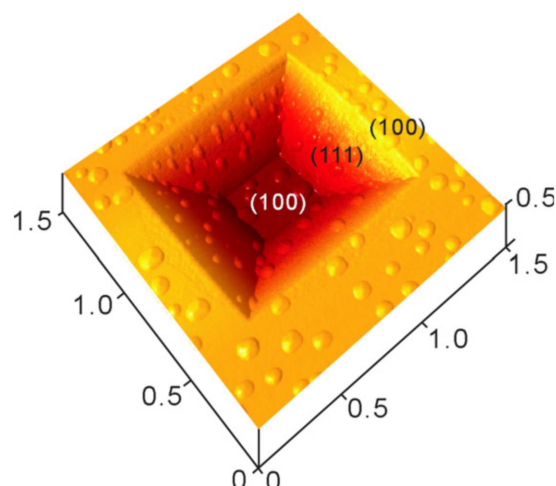

Figure 5. Three-dimensional AFM images showing a negative pyramid following Ge growth. The depletion zone is discernible on the edge of {111} facets near the (100) planes, but no such zone emerges on the border between the {111} facets. The scales are in units of micrometre.

As noted by Yang *et al*, the (100) facet near the concave edge has a low chemical potential owing to the spatially nonuniform relaxation of the strained wetting layer, and can act as a local nucleation centre. The preferred nucleation can account in part for the depletion of Ge adatoms around the nearby {111} facets, assuming that the V-groove does not impose significant diffusion barrier. Additionally, the existence of the adatom sink on the V-groove and in the pits can lead to island depletion on the (100) surface [8]. However, a separate driving force is required for depleting Ge adatoms on the {111} facet near its convex edge, a location that lacks a good sink nearby. With no other driving forces, mass transport is driven by chemical-potential gradients associated with the wetting-layer thickness [21], that is, $F = -\frac{\Delta\mu}{\Delta x}$. In addition, the diffusivity on the {111} facet is smaller than that on (100), as discussed earlier. It can be concluded that a net flux of Ge adatoms from the {111} regions toward the (100) facets indicates that the effective chemical potential μ_{100} is smaller than μ_{111}.

4. Conclusions

Nanosized surfaces with well-defined sidewall facets provide opportunities for both new methods of growth-control engineering, and also fundamental understanding of the size-dependent crystal growth phenomena during nano-island formation. Various nanosized Si{111} facets bordered by (100) planes were fabricated and Ge nano-islands were simultaneously grown on the two facets. Nano-island formation was suppressed on the {111} facets as the width of the {111} facets reduced below ∼500 nm at growth temperature

650 °C. By excluding Ge adatom sinks near the convex border of the two facets, we conclude that the effective chemical potential for Ge adatoms on the {111} facets is smaller than that on the (100) facet, resulting in an adatom flux from the {111} facets to the (100) plane. Our results provide the first direct comparison of the adatom chemical potential of two wetting layers and its influence on the growth behaviour on the nanosized surfaces.

Acknowledgments

This work was supported by the US Asian Office of Aerospace Research and Development (AOARD) under Contract No AOARD-04-4015 and in part by the National Science Council of Taiwan under Contract No NSC-94-2112-M-009-010.

References

[1] Bruce A *et al* 2005 *Quantum Dots: Fundamentals, Applications, and Frontiers* (*NATO Science Series* vol 190) (Dordrecht: Springer) and reference therein
[2] Michler P 2004 *Single Quantum Dots: Fundamentals, Applications and New Concepts* (Berlin: Springer) and reference therein
[3] Kim E S, Usami N and Shiraki Y 1999 *Semicond. Sci. Technol.* **14** 257
[4] Kitajima T, Liu B and Leone S R 2002 *Appl. Phys. Lett.* **80** 497
[5] Yang B, Liu F and Lagally M G 2004 *Phys. Rev. Lett.* **92** 25502
[6] Lee H M, Yang T H, Luo G and Chang E Y 2004 *Japan. J. Appl. Phys.* **43** L247
[7] Jin G, Lium J L, Thomas S G, Luo Y H, Wang K L and Nguyen B Y 2000 *Appl. Phys.* A **70** 551
[8] Suda Y, Kaechi S, Kitayama D and Yoshizawa T 2004 *Thin Solid Films* **464/465** 190
[9] Olzierski A, Nassiopoulou A G, Raptis I and Stoica T 2004 *Nanotechnology* **15** 1695
[10] Zhang Y Y, Zhang J, Luo G, Zhou X, Xie G Y, Zhu T and Liu Z F 2005 *Nanotechnology* **16** 422
[11] Zubel I and Barycka I 1998 *Sensors Actuators* A **70** 250
[12] Vescan L, Grimm K, Goryll M and Hollander B 2000 *Mater. Sci. Eng.* B **69/70** 324 and references therein
[13] Kim H J, Zhao Z M, Liu J, Ozolins V, Chang J Y and Xie Y H 2004 *J. Appl. Phys.* **95** 6065
[14] Szkutnik P D, Sgarlata A, Motta N and Balzarotti A 2003 *Mater. Sci. Eng.* C **23** 1053
[15] Ratto F *et al* 2004 *Appl. Phys. Lett.* **84** 4526
[16] Ratto F, Locatelli A, Fontana S, Ashtaputre S, Kulkarni S K, Heun S and Rosei F 2006 *Phys. Rev. Lett.* **96** 96103
[17] Hartmann A, Vescan L, Dieker C and Lüth H 1994 *J. Appl. Phys.* **77** 1959
[18] Motta N, Rosei F, Sgarlata A, Capellini G, Mobilio S and Boscherini F 2002 *Mater. Sci. Eng.* B **88** 264
[19] Mo Y W, Kleiner J, Webb M B and Lagally M G 1991 *Phys. Rev. Lett.* **66** 1998
[20] Kamins T I and Williams R S 1997 *Appl. Phys. Lett.* **71** 1201
[21] Tu K N, Mayer J W and Feldman L C 1992 *Electronic Thin Film Science for Electronical Engineers and Materials Scientists* (New York: Macmillan)